Archaeometry

WILEY

ORIGINAL ARTICLE OPEN ACCESS

The First Archaeomagnetic Age at Tiwanaku and Implications for Dating Andean Metallurgical Furnaces

Judit del Río[1] | Pablo Cruz[2] | Miriam Gómez-Paccard[3] | Alicia Palencia-Ortas[4] | Marina Puente-Borque[5] | F. Javier Pavón-Carrasco[5] | Erik Marsh[6]

[1]Universidad de Burgos, Laboratorio de Paleomagnetismo, Burgos, Spain | [2]UE CISOR (Unidad Ejecutora en Ciencias Sociales Regionales y Humanidades), CONICET (Consejo Nacional de Investigaciones Científicas y Técnicas), Universidad Nacional de Jujuy, San Salvador de Jujuy, Argentina | [3]IGEO (Instituto de Geociencias, CSIC-UCM), Dpto. Dinámica Terrestre y Observación de la Tierra, Madrid, Spain | [4]Universidad Politécnica de Madrid, Dpto. Ingeniería Eléctrica, Electrónica Automática y Física Aplicada, Madrid, Spain | [5]Universidad Complutense de Madrid, Dpto. Física de la Tierra y Astrofísica, Madrid, Spain | [6]CONICET, Universidad Nacional de Cuyo, Laboratorio de Paleo-Ecología Humana, Mendoza, Argentina

Correspondence: Judit del Río (jdelrio@ubu.es)

Received: 6 February 2025 | **Revised:** 8 August 2025 | **Accepted:** 29 September 2025

Funding: This work was supported by Ministerio de Ciencia e Innovación, PID2020-113316GB-100, PID2024-159020NB-100, and Consejo Superior de Investigaciones Científicas, COOPB23002.

Keywords: Andean archaeology | archaeomagnetic dating | archaeomagnetism | archaeometallurgy | furnace | pre-Hispanic Bolivia

ABSTRACT

This paper presents the first archaeomagnetic dating at Tiwanaku (Andean Altiplano). We compared the geomagnetic field values recorded by a metallurgical furnace against an updated SHAWQ2k-SH global model and a regional intensity curve, both of which include, for the first time, high-quality intensity data from the Southern Hemisphere. Results place the furnace's last use in 450–740 CE, and the decorated ceramic chronology at the site further constrains it to 570–740 CE, with maximum probability during the mid-late 600s. This marks a significant methodological advance for Andean archaeometallurgy, addressing challenges posed by thermoluminescence and radiocarbon dating in the region.

1 | Introduction

Archaeomagnetism is broadly defined as the study of the magnetic properties of archaeological materials, with archaeomagnetic dating being the most known application (Batt 2023). The latter rests on two principles. First, certain iron oxides commonly found in archaeological materials, notoriously magnetite and maghemite, acquire a permanent magnetization when they are deposited in the sediments or heated to high temperatures and then cooled back to room temperature in the presence of an external magnetic field, such as the Earth's. This temperature-induced magnetization is what we call thermo-remanent magnetization (TRM), and it records the magnetic field's characteristics existing at the time of the last heating–cooling cycle. If the archaeological material is not reheated, its magnetization remains unaltered to the present day, effectively preserving a record of the past geomagnetic field at a specific time and location. Second, the Earth's magnetic field (hereafter referred to as geomagnetic field) varies over time and space, experiencing changes in both its strength and direction. These changes occur on timescales ranging from milliseconds to millions of years; those that occur on a yearly basis or longer are known as palaeosecular variation (PSV). The accurate reconstruction of the PSV through time at different locations is the backbone of archaeomagnetic dating.

Archaeomagnetic dating entails the comparison between the intensity and direction recorded by archaeological clayey materials through a TRM with PSV reconstructions, either in the form of regional PSV curves or global geomagnetic field models. These curves and models are built from a myriad of independently dated and publicly available archaeomagnetic and

palaeomagnetic data (Brown et al. 2021). As the global database grows, so does the accuracy of archaeomagnetism as a dating technique, which benefits from more robust PSV curves that better reflect the geomagnetic field's variation. This, together with improved and easy-to-access tools (Serrano et al. 2024), open data standards (Jones et al. 2021) and a gradually richer feedback between the archaeological and geophysical communities allow for wider possibilities than just a few decades ago.

South American archaeomagnetism is quickly growing as well, both in regard of the quantity and quality of its database (Poletti et al. 2016; Gómez-Paccard et al. 2019, 2025; Goguitchaichvili et al. 2023). This study aims to evaluate whether our current understanding of geomagnetic field variations in the continent provides a solid base for archaeomagnetic dating and to apply the method to a furnace found in the outskirts of Tiwanaku (currently Bolivia). It also constitutes the first archaeomagnetic dating at this key archaeological site and, more broadly, of any pre-Hispanic Andean site—although some precedents in the region exist, such as the early works by Wolfman and Dodson (1998) and DuBois (2008) in Perú, Bowles et al. (2002) in Ecuador, and more recent studies by Lengyel et al. (2011) on several sites near Porco (Bolivian Andes). Our goal is to highlight the potential of an underutilized technique in cases when other absolute dating techniques face limitations, whether due to the nature of the archaeological finds or to its geographical particularities.

2 | Archaeological Context and the Challenges of Dating Furnaces

2.1 | Tiwanaku and the Furnace at Qatawarani

Founded during the first century CE alongside a few other major sites (Marsh 2012, 2016), Tiwanaku became a cultural and political hotspot around 600 CE. It was then that it grew into one of the major cities in the Andes, receiving an influx of population from nearby areas, possibly related to a large volcanic event (Marsh et al. 2024). Extensive domestic occupations are documented throughout the city (Couture 2003; Couture and Sampeck 2003; Janusek 2004; Marsh et al. 2023; Lémuz Aguirre 2024), and as it expanded, so did its influence on the immediate region and even more distant places in the Andes—Tiwanaku's iconic painted redware ceramics have been found at hundreds of sites, from southern Peru to northern Chile. The city collapsed by the end of the first millennium, right before a subsequent drought (Marsh et al. 2023).

At the beginning of 2023, the CIAAAT (Spanish acronym of the Archaeological and Anthropological Research Centre and Administrative Division of Tiwanaku) requested the excavation of a furnace whose north wall had already been affected by works in the neighboring field. The structure is located 570 m northeast of the plaza in Tiwanaku, in an area known as Qatawarani (16°32′54.9″ S, 68°40′42.9″ W, Figure 1).

The furnace, named QTW01, is a nearly circular construction built with neatly edged stone blocks and mortar, both intensely rubefied. The inner wall was covered with a thin layer of slaggy clay. At its uppermost level, the chamber is 2.7 × 2.8 m, with a slightly conical profile. The chamber was filled with sediment, arranged in at least three stratigraphic units, with abundant blocks of rubefied clay and pieces of melted bricks, and a cuboid carved stone measuring 51 × 37.5 × 27 cm. The ceramic production found within consists exclusively of Tiwanaku redwares. The inspection of the surrounding area yielded numerous fragments of pottery, mostly in the same Tiwanaku style, but decorated Inka Provincial, Pacajes, and Colonial wares were found in lesser numbers. The presence of numerous metal slags in the lower levels of the structure suggests that it was used in the processing of copper-bearing minerals. In this regard, potential mines are found both at the Quimsachata hills, about 10 km South of QTW01 and 75 km farther away from the site, such as those of Corocoro, Calacoto, and Don Carlos, supporting the evidence that the city of Tiwanaku would have had access to the resources required for metalworking (Macfarlane and Lechtman 2016).

QTW01 is not only the first furnace of its kind found at Tiwanaku, despite more than a century of archaeological research (Ponce Sanginés 1976), but it also stands out for its unprecedented size and constructive complexity in the region. This study aims to pinpoint when the last firing of the chamber occurred, thereby providing a *terminus ante quem* for its lifespan and offering a deeper understanding of its role within the Tiwanaku urban system. Additionally, we seek to assess the potential of archaeomagnetism as a reliable dating tool, exploring its capacity to complement other dating methods such as radiocarbon dating and thermoluminescence—which may present challenges that we will address below. We will focus on the potential of full-vector archaeomagnetic measurements to provide an accurate chronology for the existing archaeological data. This approach will not only refine the dating of the QTW01 furnace but also enhance the application of archaeomagnetic methods in other archaeological contexts, particularly those related to metallurgy and furnace use in the Andean world.

2.2 | Dating Andean Metallurgical Structures: Some Considerations

Dating archaeological contexts in the Andes relies mostly on radiocarbon and archaeological evidence. While radiocarbon dating has been crucial in unraveling the pre-Columbian history of the Americas (Macario et al. 2025), it can present particular difficulties when applied to large-scale metallurgical furnaces like QTW01. Their energy requirements are high, and in the Altiplano, only two species supply enough calorific value to operate at such a scale: the keñua tree (*Polylepis tarapacana*) and a very compact shrub, the yareta (*Azorella compacta*), widely documented in historical sources (e.g., Barba 1640). Both are very long-lived species, reaching 600–700 years in the case of keñua (Moya and Lara 2011; Solíz et al. 2009), and even more than a millennium in the case of yareta (Harpel et al. 2021). Their longevity must be considered when attempting radiocarbon dating, for a significant time lag may exist between the death of the organic matter—when atmospheric exchange of C14 stopped—and its use as fuel, which can lead to overestimates of many years, even centuries, which can steer toward older chronologies. The old-wood effect described by Schiffer (1986) is even more of a problem in furnaces, since people may have repurposed very old

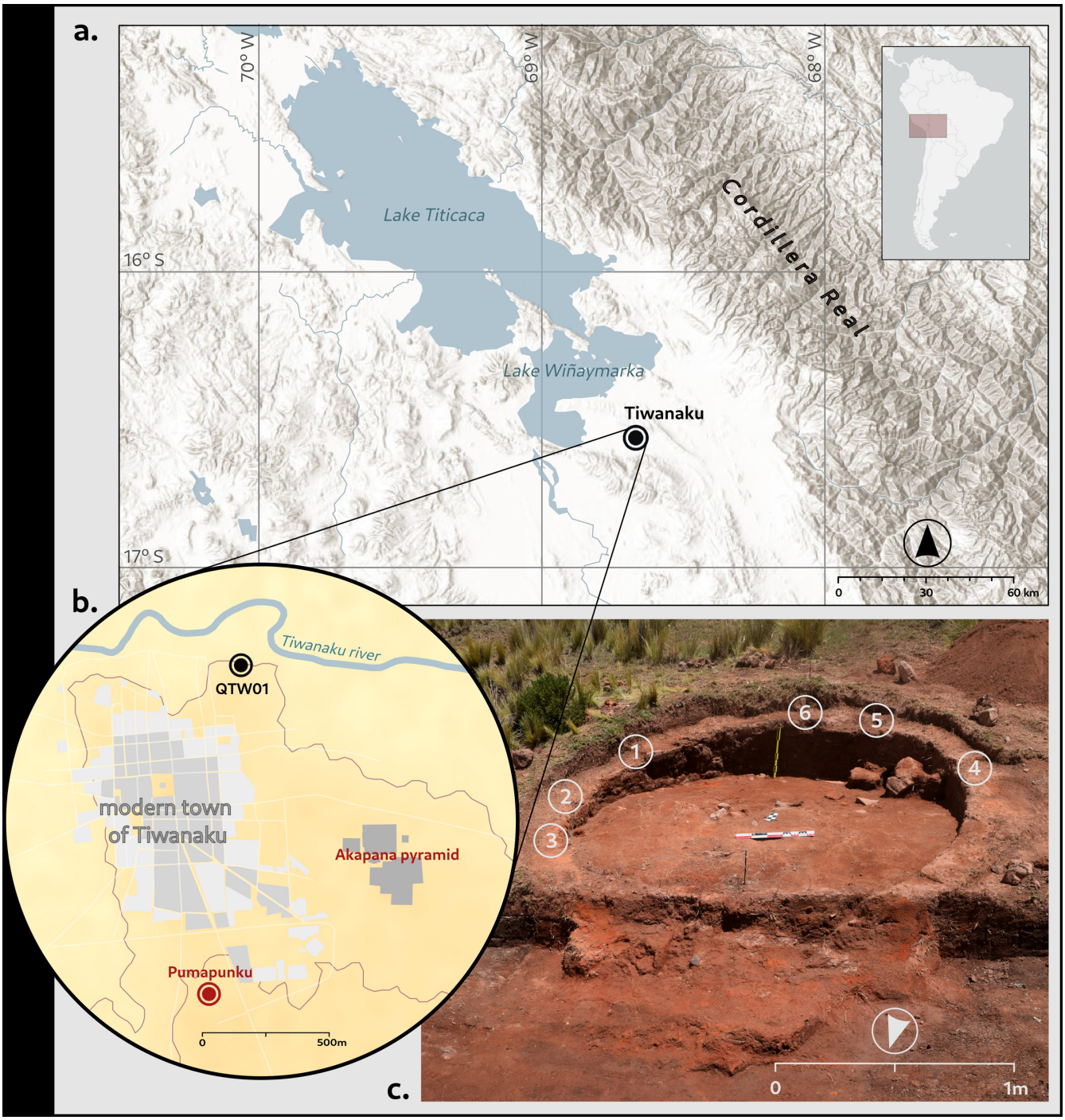

FIGURE 1 | (a) Location of Tiwanaku in the major Titicaca basin (modified from ESRI and the GIS community); (b) Location of QTW01 in relation to modern and archaeological Tiwanaku city; (c) QTW01 before excavation—numbers indicate archaeomagnetic samples.

lumber as fuel. Although some shortcuts have been proposed to circumvent this issue, such as dating in-slag charcoal, several authors point toward the possibility of older fossil charcoals getting trapped inside the metal slag, thus yielding artificially older dates (Gassman and Schäfer 2018; Vodyasov et al. 2020).

In QTW01, we face the added difficulty of the total lack of suitable materials for radiocarbon dating. The absence of charcoal inside the melting chamber comes as no surprise, given that devices such as QTW01, built to be used perennially, are routinely fired after each cycle of work in order to remove residual metal slags and contaminants that affect subsequent smelting. Additionally, the firebox, where charcoal samples would have been found, was destroyed by land remotion (Figure 1c), making sample retrieval impossible.

Luminescence techniques, such as infrared light, optical stimulation, or thermoluminescence, offer an alternative approach. While these methods are reliable in some regions, attempts to apply them to South Andean sediments, pottery, and bricks reveal important discrepancies across a range of contexts and time periods, and a disagreement with radiocarbon or historical

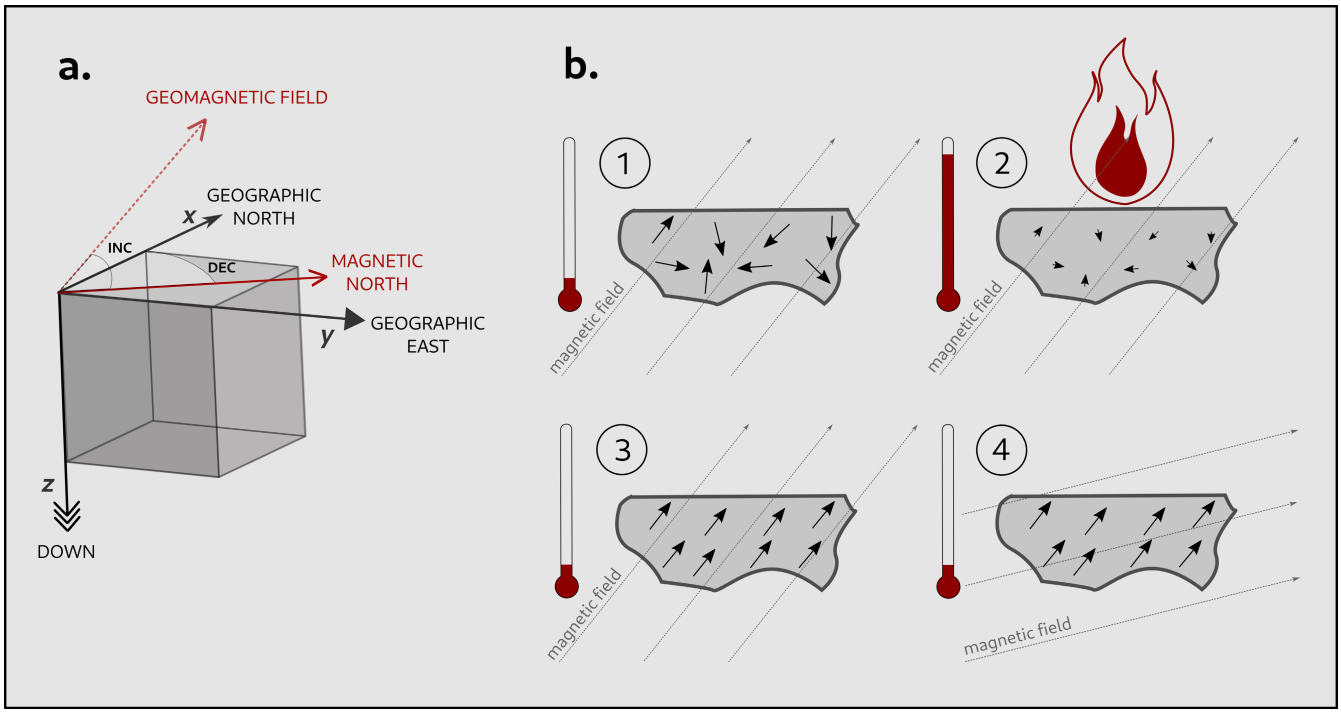

FIGURE 2 | (a) Schematic representation of a cubic specimen showing the relation between the specimen's coordinates (x, y, z) and the geomagnetic field vector. (b) Sequence showing the acquisition of a thermo-remanent magnetization (TRM) and its preservation through geomagnetic field changes. Black arrows show the direction of the acquired magnetization within the material; gray dashed lines show the direction of the Earth's magnetic field. 1. At low temperatures, the geomagnetic field does not have any significant effect on the magnetization; 2. When temperature raises, the magnetization changes toward the direction of the GMF; 3. When temperature lowers, the acquired magnetization becomes stable and preserves the direction and intensity of the GMF; 4. When the direction and/or intensity of the GMF changes, and provided the temperature is not increased again, the last-acquired magnetization remains.

dates. This may be the result of the Andes' young geology and unstable luminescence sensitivity (Marsh et al. 2021). These limitations make neither radiocarbon nor luminescence a suitable tool for dating furnaces like QTW01, and as such, we turned to archaeomagnetism as a more reliable method.

3 | Methodology

3.1 | Fundamentals of Archaeomagnetism

Before introducing the experimental workflow used to retrieve geomagnetic information from archaeological materials, we will briefly describe the behavior and geometry of the Earth's magnetic field and how archaeological structures can record its characteristics when heated.

Our geomagnetic field originates in the outer core of the planet, composed of molten iron and nickel. The geomagnetic field at any point on the Earth's surface can be represented as a vector. Figure 2a shows a schematic representation that correlates this magnetic vector with a Cartesian coordinate system, which is what allows us to describe and study the behavior of the field. In it, declination (D) is the angle between the geographic North (the point where the Earth's imaginary rotation axis intersects with the surface) and the magnetic North (the point that a compass needle aligns with), and varies between 0° and 360°. Inclination (I) is the angle between the magnetic field and a horizontal plane tangent to the Earth's surface, varying between 0° and ±90° (negative inclinations are found in the Southern hemisphere in our current geomagnetic field configuration). The intensity (B), in turn, is related to the vector's strength; current values at the surface range between ~20 and ~65 μT.

The three magnetic parameters (D, I, and B) vary through time in a nonperiodic fashion. As mentioned earlier, the long-term variation of the geomagnetic field, or PSV, is the foundation of archaeomagnetic dating. Moreover, it differs across locations, meaning that at any given point in time the field is not the same in Madrid, Tokyo, or indeed Tiwanaku. In areas within a 1000-km radius, these variations are sufficiently similar to allow the geomagnetic field to be described regionally, whereas in bigger areas, the potential differences between regions cannot be dismissed. To research the PSV and build reliable reference curves for times prior to the first direct observations from the 17th century onward—provided by marine expeditions, geomagnetic field observatories, and satellites—the only data sources are archaeomagnetic or palaeomagnetic studies of well-dated archaeological structures or rocks, which preserve the information on the geomagnetic field's direction and intensity in the stable magnetic record acquired during the last heating event or rock formation.

The geomagnetic field leaves its imprint in archaeological and geological materials due to the iron minerals they contain, mainly oxides such as magnetite, maghemite, or hematite, which can acquire a permanent magnetization. One such way of becoming magnetized is through exposure to high temperatures.

For example, when a furnace is heated—whether to fire pottery, bricks, or to refine ores—the magnetization of the iron oxides changes, aligning with the current geomagnetic field. When the furnace cools, the last-acquired magnetization becomes fixed, acting like minuscule compass needles within the materials that remain stable through time—unless they are heated again to the same or higher temperatures (Figure 2b). We call this process TRM. The unadulterated magnetization acquired in the past is termed natural remanent magnetization (NRM) and can be retrieved at the laboratory through specific experimental protocols.

The acquisition of a permanent magnetization has to contend with some physical phenomena that should be taken into account at the laboratory. One of them is the anisotropy of thermo-remanence: the preferential alignment of iron oxides along the easy axis of magnetization within the crystal lattice, which makes it more efficient to become magnetized, energetically speaking. This effect is quite common in archaeological materials such as wheel-thrown or coil-formed (Jones et al. 2020) ceramic wares, as the constant manipulation of clay affects the arrangement of iron minerals. A recent study by Palencia-Ortas et al. (2021) shows that this effect can lead to potential biases in the estimation of the ancient direction of the geomagnetic field. Another significant factor is the cooling rate (CR), i.e., the speed at which the materials cool, which may affect the degree and nature of the acquired TRM, and consequently the results obtained at the laboratory. The most up-to-date quality standards in archaeomagnetism consider the correction of these unwanted effects. The process of magnetization is, in reality, more intricate and is also influenced by other factors such as mineralogy, magnetic domain size, and magnetic granulometry. For a comprehensive explanation of the physical mechanisms of magnetization, the reader is referred to Tauxe et al. (2018).

3.2 | Field Sampling, Specimen Preparation, and Laboratory Work

We retrieved six oriented samples from the walls of the circular kiln, distributed along its perimeter (Figure 1c). This requires the creation of a horizontal surface atop the sample by pouring liquid plaster over it and leveling it with the help of a methacrylate plate and a bulls-eye spirit while still malleable. After it dries, the azimuth line is marked on the surface. We used a double orientation protocol with both magnetic and solar compasses—the former produces a mark aligned with the magnetic North, the latter provides the direction of the Sun, which, when paired with the exact hour and the geographical coordinates, allows for the reconstruction of its original position. Each sample is then detached from its original place, thus preserving the original orientation. Once in the lab, the samples are consolidated using a solution of sodium silicate, a common archaeomagnetic hardening agent, before being set in a cubic plaster mold to achieve a regular shape and subsampled to obtain standardized ~8 cm^3 cubic specimens (the full list is available in the Supporting Information [SI] Section I).

Archaeomagnetic studies usually involve two types of experiments: rock magnetism analyses, which aim to identify the iron mineral responsible for the GMF record, and experiments focused on determining the direction and intensity of said field. In our case, rock magnetism comprised a standardized set of experiments designed to provide a comprehensive understanding of the magnetic properties of the materials, which is crucial for an accurate interpretation of the archaeomagnetic data. Those experiments were as follows:

- the measurement of the initial magnetic susceptibility (χ) of the specimens, which provides some information about their characteristics before they undergo further analysis;
- an isothermal remanent magnetization (IRM) acquisition curve, which helps to assess the ability of the specimen to acquire a stable remanent magnetization under constant temperature conditions;
- a backfield curve, used to determine the coercivity of the magnetic minerals (the ability to resist an external magnetic field without becoming demagnetized);
- a hysteresis loop, which provides information about the magnetic behavior of the materials with a changing field, including their remanent magnetization and coercivity; and
- a thermomagnetic curve, which measures the changes in magnetization as a function of temperature revealing the thermal stability of the minerals.

Archaeointensity and archaeodirectional determinations were obtained through the classic Thellier and Thellier (1959) protocol, based on the progressive erasure of the originally acquired NRM and its substitution with an experimentally induced magnetization (artificial TRM), and included additional experimental steps, such as partial TRM checks to monitor possible magnetization changes due to thermal treatment, and corrections for the effects of the TRM anisotropy (TRMani) and CR. The latter is crucial to correct the potential distortion of data due to these effects and provide more accurate results. The mean intensity was derived from only high-quality determinations and is provided as a weighted mean with its standard deviation. Additional directional data were obtained from the stepwise thermal demagnetization of 18 specimens. Mean values for the declination and inclination were calculated using Fisher statistics (Fisher 1953), based on data from both the Thellier and thermal demagnetization experiments. The mean direction is reported with its associated α95 value—the cone of confidence within which the direction is determined at 95% probability. Further details can be found in SI Sections II and III.

3.3 | Elements of Archaeomagnetic Dating

Once the full-vector values are obtained—i.e., the mean declination, inclination, and intensity values of all specimens and samples—we can compare them with the behavior of the geomagnetic field through time as described in reference PSV curves. It follows, then, that the uncertainties of said reference curves are critical. As with other methods such as radiocarbon, the accuracy of archaeomagnetic dating strongly depends on the precision of the reference curve used. The precision of said curve, in turn, depends on the quantity and quality of the data used to build it, the spatiotemporal distribution of said data,

and the uncertainties inherent to them. In addition, the rate of change plays a significant role: periods of slower geomagnetic changes result in broader dating intervals (causing a plateau effect), while periods of more rapid fluctuations yield more precise chronologies, again similar to what happens with radiocarbon curves. Furthermore, larger uncertainties in the experimental determination of the mean direction and intensity will also lead to a broader age range—for more details, see Pavón-Carrasco et al. 2011).

Given the above considerations, it is best practice in archaeomagnetic dating to use a geomagnetic field reconstruction as refined as possible to account for fine-scale regional changes of the field in the study area, and we have approached the dating of QTW01 in such a way. High-resolution regional PSV curves are the most reliable option when the amount of archaeomagnetic data in the target region is enough, providing a well-constrained evolution of the geomagnetic field through time. If the region is characterized by an important lack of archaeomagnetic data, such as South America is, no PSV curves are well defined for dating purposes, and global field palaeoreconstructions can be employed as an alternative. In the latter case, a local PSV curve is synthesized from the global model and is used for dating. Considering the best available options for Tiwanaku, we compared our experimental data against two global models and two regional PSV curves, the rationale of which we will address in depth in the discussion.

We used ArchaeoPyDating (Serrano et al. 2024), a user-friendly, Python-based free software that calculates combined probability density functions (PDFs) based on the statistical correlation between the geomagnetic information recorded by the target structure and that given by the reference PSV curve. In other words, it determines the likelihood of all different geomagnetic field parameters appearing in the reference curves used. The results are usually provided as a probability range over a span of time at a given level of confidence (1σ, 68%, and 2σ, 95%). See Serrano et al. (2024) for more details.

4 | Results and Discussion

4.1 | The Archaeomagnetic Record of QTW01

The first step in the experimental pipeline is to explore the magnetic mineralogy of the specimens and assess their suitability for archaeomagnetic studies. The initial NRM values for all studied specimens range from 3.4E-04 Am^2/kg to 8.5E-03 Am^2/kg. We plotted them against the initial mass normalized magnetic susceptibility (ranging from 5.3E-07 m^3/kg to 5.5E-06 m^3/kg) to obtain the Koenigsberger ratio, or Q_n (Koenigsberger 1930). This parameter serves as a proxy to infer thermal treatment in the samples—materials heated to high temperatures are prone to display higher Q_n values (Stacey 1967)—, which is why it is also called elsewhere fire efficiency ratio (Di Chiara et al. 2021). The specimens consistently appear above the 10 threshold line (Figure 3a), which provides a solid lead to think that the material was well heated at the moment it acquired a magnetization, in agreement with the function of the structure as a firing kiln. As such, the material is very well suited for archaeomagnetic analyses.

The parameters derived from rock magnetism experiments point to a great homogeneity in the magnetic mineralogy of the specimens. The IRM acquisition and backfield curves show that most of the specimens are entirely saturated at low magnetic fields (~300 mT). Figure 3b displays two representative specimens with slightly different characteristics—note how specimen *bot19* shows higher magnetization values and runs at a light upward slope compared to *bot08*. The same behavior can be seen on their backfield curves (Figure 3b). Hysteresis cycles, of which we show again two representative specimens in Figure 3c, yield well-defined loops, with their upper and lower branches closing neatly, almost no paramagnetic or diamagnetic fraction, saturation magnetization (Ms) values ranging from 8.8E-02 Am^2/kg to 5.8E-01 Am^2/kg, and remanent saturation magnetization (Mrs) values between 7.3E-03 Am^2/kg and 2E-01 Am^2/kg. Lastly, the thermomagnetic curves are highly reversible for all specimens and display Curie temperatures ranging from 520°C to 598°C, with most of them clustered around 540°C. In the example presented in Figure 3d, again the specimen *bot19* shows higher magnetization values than its counterpart *bot08*. For additional plots, refer to SI Section III.

All in all, the magnetic mineralogy is ruled by a low-coercivity mineral, as revealed by its small coercive fields and quick saturation. Curie temperatures slightly lower or higher than 580°C (the standard for pure magnetite) point to a magnetite phase with very low titanium substitution in the former case and a mildly oxidized magnetite in the latter, both of which are among the most common magnetic carriers in archaeological materials.

In a second phase, 12 specimens underwent Thellier–Thellier palaeointensity experiments. Figure 4 shows typical Arai plots for some of them, alongside their corresponding Zijderveld plots, the intensity value corrected for anisotropy and CR effects (Bac), and the quality parameter (q), which is used as an indicator of the reliability of the experiments—the higher the q value, the more robust the paleointensity determination.

The Arai plots invariably reveal a single component defined between 150°C and the end of the vector, 490°C in some cases and 570°C in others. The majority of specimens carry no viscous component, although a timid curvature can be seen in the first thermal steps in some specimens (Figure 4b,d), disappearing at 150°C–200°C. No chemical alterations due to heating at the end of the slope are perceptible either, and the pTRM checks regularly coincide with their original temperature by ±10% of their value. The minimum number of steps used in the calculation of the slope is 9, which encompasses at least 70% of the magnetization of the specimen as expressed by f, ranging from 0.72 to 0.96. The curvature parameter k ranges from −0.09 to 0.26, β between 0.01 and 0.04, and the quality parameter q runs from 20.9 up to 111.8. MAD (2.7°–5.1°), and DANG (0.2°–2.5°) values for all 12 specimens are well within the threshold set for these criteria, the exception being specimen *bot27*, for which DANG = 5.1°. However, as every other quality criterion is in range and even exceeds expectations ($n = 9$, $f = 0.7$, $q = 62.4$), we chose to include it in the calculations.

The strict selection criteria are similar to those used in our previous studies (e.g., Bonilla-Alba et al. 2024, 2021) and have been applied to preserve only the most reliable results. Further

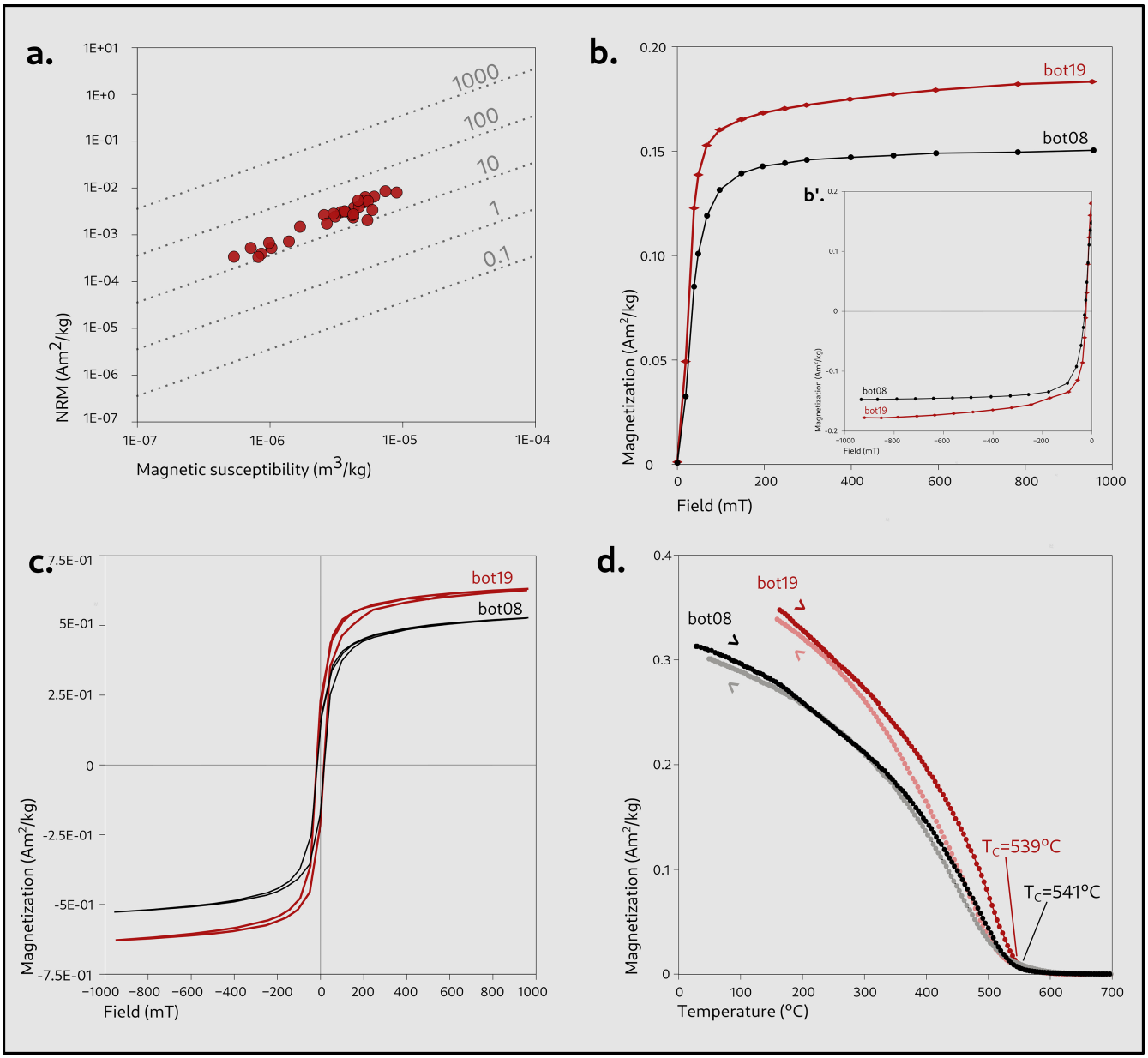

FIGURE 3 | (a) Koenigsberger ratio for all measured specimens, with susceptibility plotted in the abscissa and initial NRM values in the ordinate. (b) IRM acquisition curves of two representative specimens plotted side to side for comparison, bot08 (in black) and bot19 (in burgundy). (b′) Backfield curves. (c) Hysteresis loops. (d) Temperature vs. magnetization curves; the bright colors (black, burgundy) represent the heating cycle; the muted colors (gray, pink) the cooling cycle.

development of this topic is beyond the scope of this paper, but details about the protocol followed can be found in the supplementary material (see SI Section III for the applied quality criteria and SI Section IV for all intensity data at the specimen, sample, and site level.

From the intensity estimates at the specimen level, we calculated the mean intensity recorded by QTW01. The uncorrected values yield an intensity of $B = 47.1 \pm 4.3$ μT. The anisotropy-only corrected value shows a very slight decrease of $Ba = 45.5 \pm 4.6$ μT, which demonstrates that, as expected for this kind of structure, the TRMani does not have a significant effect. The values obtained after both TRMani and CR corrections ($Bac = 41.9 \pm 4.8$ μT), on the other hand, show a decrease of almost 6μT, which, although still a low fluctuation, proves the importance of such tests for an accurate intensity determination. Note that we provide the intensity value as a weighted mean (Prévot et al. 1985), a calculation that takes into account the quality of each datum; the full table with standard means can be found in SI Section IV.

Archaeodirections were averaged from the Thellier–Thellier demagnetized specimens, using the same temperature range chosen for the calculation of the intensity, plus the extra directions obtained from the 18 specimens that were thermally demagnetized. To determine the declination and inclination values at the specimen level, we calculated the vector anchoring it to the origin of coordinates—although, due to the extreme linearity of the plots, the difference between doing so and calculating the direction without forcing the component is of no significance. Additional demagnetization plots can be found in SI Section V.

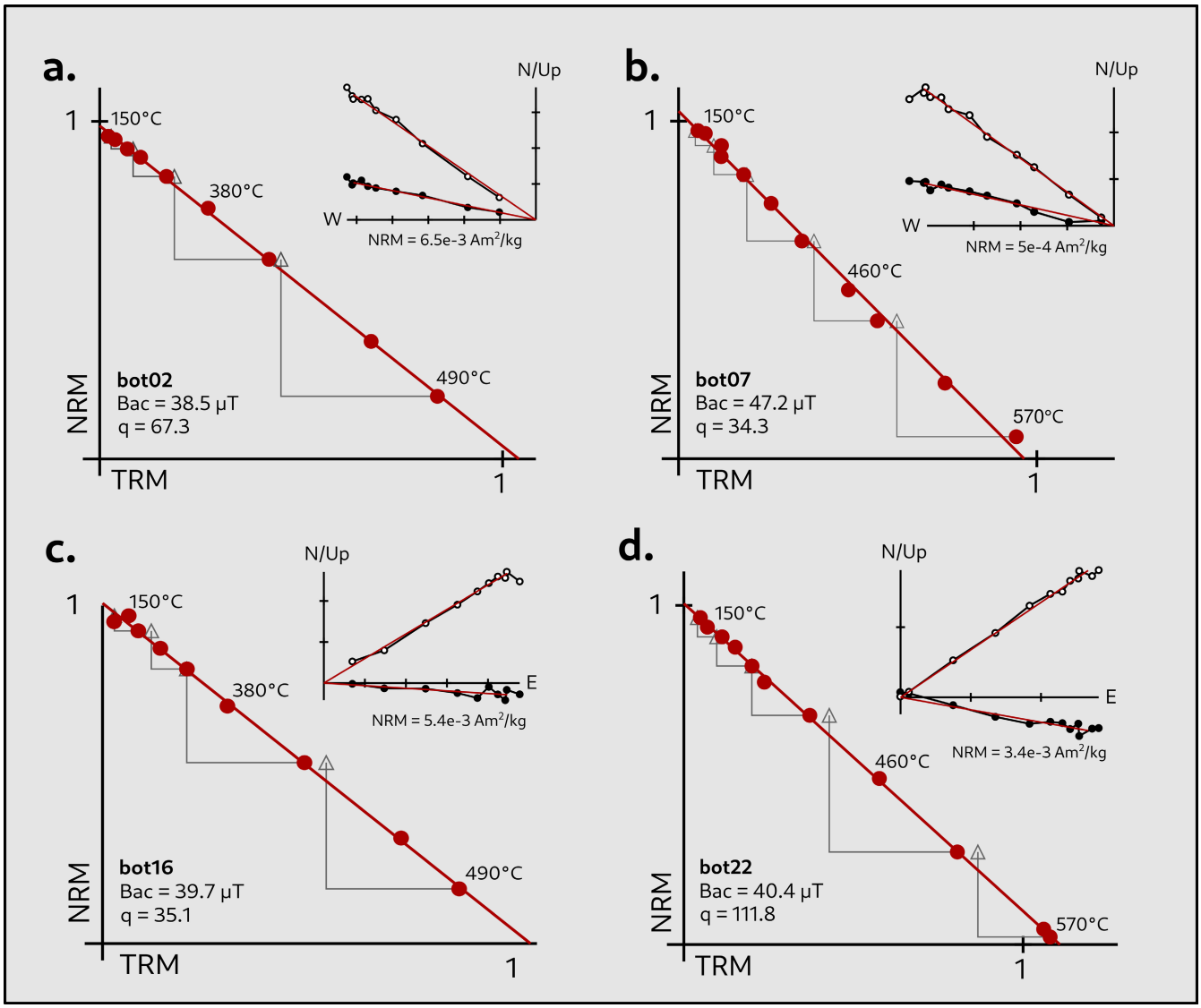

FIGURE 4 | Representative Arai (intensity) plots for specimens belonging to different samples, including their related Zijderveld (directional) plots. Red lines in Arai plots mark the sequence of temperature steps used in intensity calculations; gray arrows mark the pTRM checks. The values of the obtained intensity at the specimen level corrected for anisotropy and cooling rate effects (Bac) and the quality parameter (q) are provided, alongside the initial NRM values.

Unlike intensity, which is not affected by mistakes in in situ orientation, directional determinations greatly depend on the correct orientation of each collected sample. To minimize potential errors during field orientation, we preserved the hierarchical structure to obtain the final mean direction, progressing from the specimen to the sample to the full furnace, and calculating the averaged direction at each level (Table S1 Section V). While not all specimens used for directional calculations could be corrected for TRMani and CR variations, those that underwent the Thellier protocol did. The comparison of directions obtained from each group (Thellier–Thellier and thermally demagnetized) reveals an obvious offset concerning especially the declinations, whose uncorrected values overestimate the mean declination of the furnace by an average of 5.2°. When considering the data at the specimen and sample levels, these differences are even more dramatic, reaching in some cases more than 10°. The uncorrected inclination values differ only by 1.5° from corrected values. As such, we deemed the TRMani and CR effects to have notably affected the geomagnetic field record in the furnace, and we only retained the TRMani and CR corrected directional values. To date the furnace, thus, we employed the corrected full-vector values (Bac = 41.9 ± 4.8 μT, D = 3.2°, I = −35.4°, α95 = 2.1°, α95 = 2.1°).

4.2 | Dating QTW01

As hinted previously, in order to obtain reliable dating results the selection of appropriate reference curves is critical. Although the ideal approach would involve the use of regional PSV curves based on a substantial amount of robust and well-distributed data across time and space, no such data are currently available for Tiwanaku. Previous research on South America (Poletti et al. 2016; Gómez-Paccard et al. 2019; Goguitchaichvili et al. 2023) has proven that the quantity and

quality of archaeomagnetic data remain insufficient to build regional reference curves. Recent studies conducted by our group, however, have provided the first nearly-continuous intensity curve for Northwest Argentina based only on high-quality archaeomagnetic data for the last two millennia (Gómez-Paccard et al., forthcoming). This new intensity PSV curve, located originally at 31° S, 60° W, can be relocated to our target location and used to date QTW01.

Regarding the field's directional parameters, i.e., declination and inclination, the lack of regional data for Bolivia and neighboring areas forces us to rely exclusively on global palaeomagnetic field models. Although several global models have been published in the past decade, none have been definitively proven to reproduce with full accuracy the geomagnetic field's behavior in South America. Maximiano et al. (2024) recently proposed the combination of different global models —namely, BIGMUDI (Arneitz et al. 2017, 2019), Arch3k (Korte et al. 2009), and SHAWQ2k (Campuzano et al. 2019)— as the best option for dating in the continent. However, all of them include only a very limited amount of high-quality data for South America, as highlighted in critical reviews of the South American archaeomagnetic database (Poletti et al. 2016; Gómez-Paccard et al. 2019; Goguitchaichvili et al. 2023). To address these limitations, Gómez-Paccard et al. (forthcoming) updated the SHAWQ2k global model by incorporating the newly obtained intensity data from NW Argentina for the last 2000 years, in addition to other recent directional and intensity data for the Southern Hemisphere not included in the previous model (such as those in Turner et al. 2020; see Brown et al. 2021 for a systematic review of archaeomagnetic datasets). Another critical argument for the use of the SHAWQ2k is the fact that this model is the only one that includes a hierarchical weighting of the data based on their quality. In it, an archaeomagnetic datapoint contributes with a higher weight to the global geomagnetic field characterization the higher its quality (for details, see Campuzano et al. 2019). In the following paragraphs, we refer to the updated version of Gómez-Paccard et al. as SHAWQ2-SH (Gómez-Paccard et al., forthcoming).

Taking all this into account, we dated the furnace using the following four different combinations of PSV curves, all relocated at Tiwanaku's coordinates:

1. Declination, inclination, and intensity PSV curves provided by the original SHAWQ2k global model
2. Declination and inclination curves from SHAWQ2k and the local intensity PSV curve of Northwest Argentina
3. Declination, inclination, and intensity provided by the updated SHAWQ2k-SH global model
4. Declination and inclination curves from the updated SHAWQ2k-SH and the local intensity PSV curve of Northwest Argentina

The dating results at 68% and 95% confidence are summarized in Table 1.

For illustration purposes, we provide a graphical representation of the dating obtained with the declination and inclination from SHAWQ2k-SH and the intensity PSV from the Argentinian curve at 95% confidence, combination No. 4 above. Figure 5a–a′ shows the stereogram with the direction obtained from QTW01 and the decomposition of the full geomagnetic vector (*D*, *I*, and *B*). In a′, the thick black lines with translucent gray error bands represent the values of declination, inclination, and intensity retrieved from the furnace; the maroon lines and bands represent the variation of those same parameters through time, as per SHAWQ2k-SH and the Argentinian PSV intensity curve. At the bottom of each graph, the gray areas represent the PDF for each parameter at 95% confidence, marked by the dashed black line. Figure 5b shows the chronology provided by ArchaeoPyDating. The combined PDF of declination, inclination, and intensity for combination No. 4 suggests three possible times for the furnace's last use: 1–205 CE, 450–740 CE, and 1485–1705 CE. All dating approaches at 2σ (Table 1 and S1 Section VII) return three similar age intervals.

TABLE 1 | Archaeomagnetic dates at 68% and 95% confidence, obtained from the global models and the Argentinian intensity PSV curve.

	1σ (68%)	2σ (95%)
SHAWQ2k	1–120 CE	1–165 CE
	510–525 CE	460–755 CE
	630–735 CE	1490–1690 CE
D and *I* (SHAWQ2k) + intensity (local NW Argentina curve)	15–135 CE	1–205 CE
	515–545 CE	450–740 CE
	620–705 CE	1485–1705 CE
SHAWQ2k-SH	155–285 CE	1–320 CE
	720–790 CE	545–600 CE
		645–825 CE
D and *I* (SHAWQ2k-SH) + intensity (local NW Argentina curve)	20–130 CE	1–205 CE
	515–545 CE	450–740 CE
	620–705 CE	1485–1705 CE

To assess which time range is most likely, we return to the archaeological evidence found at QTW01. The earliest age (1–205 CE, as per results in Figure 5) is quite unlikely, since the earliest human occupation at Tiwanaku is estimated along the second century CE. This is illustrated in Figure 5c, which shows the estimated population events at Tiwanaku during the first millennium CE (updated from Marsh (2012), alongside cultural markers in the archaeological record such as the presence of redwares or the reported age of the church's construction. The youngest range (1485–1705 CE) overlaps with the Colonial period. Spanish activity in Tiwanaku is clear by the 1570s (Guengerich and Janusek 2021), and a church was built before 1600 (Lizárraga 1605/1916). Although some blocks taken from monuments from the Tiwanaku period were repurposed in the construction of the church, archaeological evidence leads us to believe that this monumental project probably did not involve QTW01, since the bricks found in the furnace are not Colonial in style, and there were no other Colonial artifacts in or around the furnace.

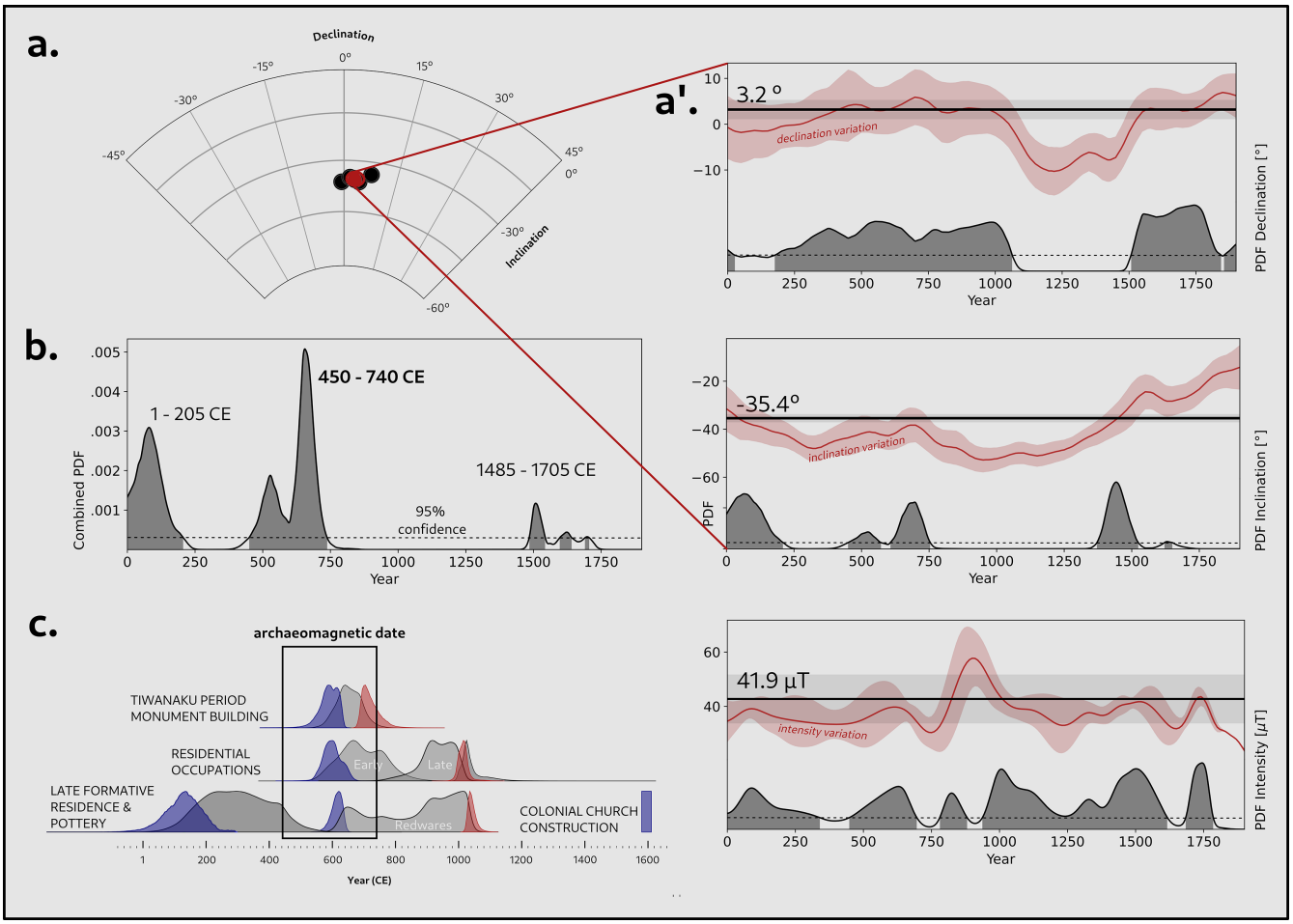

FIGURE 5 | (a) Stereographic projection of the archaeodirection recorded by QTW01. (a′) Full-vector geomagnetic field values (declination, inclination, and intensity). (b) Date obtained from directional data from SHAWQ2K-SH and Argentinian PSV curve at 95% probability; the bold interval constitutes our proposed date considering archaeological evidence. (c) Available radiocarbon dates for different occupational phases at Tiwanaku (after Marsh et al. 2023), with the obtained archaeomagnetic age superimposed for comparison; blue curves represent beginning boundaries, red curves end boundaries, and gray-shaded areas the estimates that summarize each set of radiocarbon dates. Note that the horizontal axes in (b) and (c) run at different scales.

In contrast, archaeological evidence agrees strongly with the central interval (450–740 CE). This date is compatible with the carved block found in the furnace, similar to those from the Pumapunku (Vranich 2006; Figure 1b), one of Tiwanaku's main monuments built around ~580–710 CE (Marsh et al. 2023). The redwares found within the chamber and on the surrounding area are an even more reliable temporal marker: they have appeared in 42 other contexts at Tiwanaku with associated radiocarbon dates, which suggests that this style was discarded from ca. 620–1040 CE (Figure 5c, medians from the Bayesian models in Marsh et al. 2023). Hence, unless these are exceptionally early redwares, they likely postdate the starting boundary (whose median lies at ~620 CE and its 95% probability range at 570–650 CE). As the archaeomagnetic dating suggests a date no later than 740 CE, this brackets the likely final firing of the furnace, with the peak probability during the mid to late 600s CE.

Despite small variations of a few decades, the differences between all reference models/curves in the four combinations are minimal. The inherent smoothing of global models hinders a more accurate dating of the QTW01 furnace for the moment being, but when refined full-vector local PSV curves become available, the archaeomagnetic dating could be narrowed down. We therefore propose that QTW01 was last fired in the span ranging from 570 to 740 CE, considering the 95% probability distributions for both redwares and the archaeomagnetic dating. However, the probability peaks in the mid to late 600s CE, currently our best estimate for when the furnace was last fired. This took place during the Early Tiwanaku phase (Figure 5c), when new residents and itinerant workers built two major monuments, the Akapana pyramid and Pumapunku, contributing to the monumentalization of the city and making Tiwanaku one of the Andes' most remarkable places, with a far-reaching fame that lasted for centuries.

The results obtained from our archaeomagnetic analysis go beyond the dating of this particular structure. As previously discussed, metallurgical furnaces pose difficulties to radiocarbon and thermoluminescence dating, some of which are impossible to overcome. This study proves that archaeomagnetism can be an effective tool to determine the age of furnaces,

kilns, and other similar remains that reached high temperatures during their last use. However, in order to fully benefit from the method, robust regional PSV curves are needed. Achieving this will require the improvement of the South American database by retrieving archaeomagnetic data from well-dated furnaces and kilns in the area. A more populated pool of regional data will not only increase our understanding of fascinating geophysical features such as the South Atlantic Anomaly and other traits of the ancient field's behavior at a regional scale, but will also enhance the possibilities that archaeomagnetic dating offers in the continent.

5 | Conclusions

This paper reports the first archaeomagnetic dating at Tiwanaku and in the Titicaca basin. We analyzed 30 specimens belonging to six oriented samples from an ore-reducing furnace, applying anisotropy of the TRM and CR corrections at the specimen level. We compared the geomagnetic field values recorded by the structure against two global geomagnetic field models and two local PSV curves, which suggest that the furnace was last used between 450 and 740 CE, dated at 95% confidence. By comparing dates for the associated ceramics, we can narrow the likely range to 570–740 CE (95%). The age is coeval with the start of monumental construction work (the Akapana and Puma Punku) at Tiwanaku. The accuracy of archaeomagnetic dating, based on the last high-temperature combustion event, provides a solution to potential pitfalls in radiocarbon and luminescence dating in the region, emphasizing its value for pre-Hispanic Andean archaeology. Furthermore, our results highlight the need of refining a local PSVC in central South America, an area that holds significant potential for both geomagnetic and archaeometallurgical research.

Acknowledgments

The authors are sincerely grateful to Dr. S. A. Jones and an anonymous reviewer for the time invested in this manuscript. Their suggestions improved the final article's readability and clarity; any remaining mistakes are the author's alone. This work was funded by projects PID2020-113316GB-100 "SUMATE" (Spanish Ministry of Science, Innovation and Universities), PID2024-159020NB-100 "GEOFISICA" (Spanish Ministry of Science, Innovation and Universities), and COOPB23002 (CSIC). We thank the excellent work and kind spirits of Aída Adsuar at the lab. P.C. acknowledges Marc Pouilly (Institut de Recherche pour le Développement) and Luis Miguel Callisaya (CIAAT) for their logistic support in the field. J.d.R. acknowledges the privilege of working at Tiwanaku and thanks her coauthors and her support network, always unwavering.

Conflicts of Interest

The authors declare no conflicts of interest.

Data Availability Statement

The archaeomagnetic data reported in this article are linked to the following MagIC contribution: https://earthref.org/MagIC/20489. Additionally, raw and processed data can be found at 10.5281/zenodo.14749829. The SHAWQ2k model (Campuzano et al. 2019) is available at https://earthref.org/ERDA/2453/.

References

Arneitz, P., R. Egli, R. Leonhardt, and K. Fabian. 2019. "A Bayesian Iterative Geomagnetic Model With Universal Data Input: Self-Consistent Spherical Harmonic Evolution for the Geomagnetic Field Over the Last 4000 Years." *Physics of the Earth and Planetary Interiors* 290: 57–75. https://doi.org/10.1016/j.pepi.2019.03.008.

Arneitz, P., R. Leonhardt, E. Schnepp, et al. 2017. "The HISTMAG Database: Combining Historical, Archaeomagnetic and Volcanic Data." *Geophysical Journal International* 210, no. 3: 1347–1359. https://doi.org/10.1093/gji/ggx245.

Barba, Á. A. 1640. *Arte de los Metales, en Que se Enseña el Verdadero Beneficio de los de Oro, y Plata por Azoque: El Modo de Fundirlos Todos, y Como se Han de Refinar, y Apartar Unos otros*. Imprenta del Reyno.

Batt, C. 2023. "Archaeomagnetic Dating." *Handbook of Archaeological Sciences* 1: 99–117.

Bonilla-Alba, R., M. Gómez-Paccard, F. J. Pavón-Carrasco, et al. 2024. "First Full-Vector Archeomagnetic Data From Central Asia (3 BCE to 15 CE Centuries): Evidence for a Large Non-Dipole Field Contribution Around the First Century BCE." *Journal of Geophysical Research: Solid Earth* 129, no. 2: e2023JB027910. https://doi.org/10.1029/2023JB027910.

Bonilla-Alba, R., M. Gómez-Paccard, F. J. Pavón-Carrasco, et al. 2021. "Rapid Intensity Decrease During the Second Half of the First Millennium BCE in Central Asia and Global Implications." *Journal of Geophysical Research: Solid Earth* 126, no. 10: e2021JB022011. https://doi.org/10.1029/2021JB022011.

Bowles, J., J. Gee, J. Hildebrand, and L. Tauxe. 2002. "Archaeomagnetic Intensity Results From California and Ecuador: Evaluation of Regional Data." *Earth and Planetary Science Letters* 203, no. 3: 967–981. https://doi.org/10.1016/S0012-821X(02)00927-5.

Brown, M. C., G. Hervé, M. Korte, and A. Genevey. 2021. "Global Archaeomagnetic Data: The State of the Art and Future Challenges." *Physics of the Earth and Planetary Interiors* 318: 106766. https://doi.org/10.1016/j.pepi.2021.106766.

Campuzano, S. A., M. Gómez-Paccard, F. J. Pavón-Carrasco, and M. L. Osete. 2019. "Emergence and Evolution of the South Atlantic Anomaly Revealed by the New Paleomagnetic Reconstruction SHAWQ2k." *Earth and Planetary Science Letters* 512: 17–26. https://doi.org/10.1016/j.epsl.2019.01.050.

Couture, N. C. 2003. "Ritual, Monumentalism, and Residence at Mollo Kontu, Tiwanaku." In *Tiwanaku and Its Hinterland: Archaeological and Paleoecological Investigations of an Andean Civilization, Vol. 2: Urban and Rural Archaeology*, edited by A. L. Kolata, 202–225. Smithsonian Institution Press.

Couture, N. C., and K. Sampeck. 2003. "Putuni: A History of Palace Architecture at Tiwanaku." In *Tiwanaku and Its Hinterland: Archaeological and Paleoecological Investigations of an Andean Civilization, Vol. 2: Urban and Rural Archaeology*, edited by A. L. Kolata, 226–263. Smithsonian Institution Press.

Di Chiara, A., L. Tauxe, T. E. Levy, M. Najjar, F. Florindo, and E. Ben-Yosef. 2021. "The Strength of the Earth's Magnetic Field From Pre-Pottery to Pottery Neolithic, Jordan." *Proceedings of the National Academy of Sciences* 118, no. 34: e2100995118. https://doi.org/10.1073/pnas.2100995118.

DuBois, R. L. 2008. "Geomagnetic Results, Secular Variation, and Archaeomagnetic Chronology, United States and Mesoamerica." In *Including Archaeomagnetic Data and Time Assignments (No. 2008)*. Oklahoma Geological Survey, University of Oklahoma.

Fisher, R. A. 1953. "Dispersion on a Sphere." *Proceedings of the Royal Society of London* 217, no. 1130: 295–305. https://doi.org/10.1098/rspa.1953.0064.

Gassman, G., and A. Schäfer. 2018. "Doubting Radiocarbon Dating From In-Slag Charcoal: Five Thousand Years of Iron Production at Wetzlar-Dalheim?" *Archeologické Rozhledy* 3, no. LXX: 309–327. https://doi.org/10.35686/ar.2018.14.

Goguitchaichvili, A., R. García-Ruiz, C. Greco, et al. 2023. "Evolution of the Earth's Magnetic Field Strength in Northwestern Argentina During the Last Two Millennia: Towards the Improvement of South American Geomagnetic Paleosecular Variation Curve." *Journal of South American Earth Sciences* 126: 104357. https://doi.org/10.1016/j.jsames.2023.104357.

Gómez-Paccard, M., A. Chauvin, M. E. Albeck, et al. 2019. "New Archeointensity Data From NW Argentina (1300–1500 CE)." *Physics of the Earth and Planetary Interiors* 286: 92–100. https://doi.org/10.1016/j.pepi.2018.11.004.

Gómez-Paccard, M., A. Chauvin, R. Bonilla-Alba, C. Vidal-Lorenzo, and M. Salas. 2025. "Archaeointensity Study of Pottery From the Maya Settlements of La Blanca and Chilonché (Petén, Guatemala): New Data to Constrain the Geomagnetic Field Evolution in Central America." *Physics of the Earth and Planetary Interiors* 362: 107343. https://doi.org/10.1016/j.pepi.2025.107343.

Guengerich, A., and J. W. Janusek. 2021. "The Suñawa Monolith and a Genre of Extended-Arm Sculptures at Tiwanaku, Bolivia." *Ñawpa Pacha* 41, no. 1: 19–46. https://doi.org/10.1080/00776297.2020.1830974.

Harpel, C. J., C. Kleier, and R. Aguilar. 2021. "Azorella Compacta's Long-Term Growth Rate, Longevity, and Potential for Dating Geomorphological and Archaeological Features in the Arid Southern Peruvian Andes." *Journal of Arid Environments* 188: 104470. https://doi.org/10.1016/j.jaridenv.2021.104470.

Janusek, J. W. 2004. "Tiwanaku and Its Precursors: Recent Research and Emerging Perspectives." *Journal of Archaeological Research* 12, no. 2: 121–183. https://doi.org/10.1023/B:JARE.0000023711.96664.1b.

Jones, S. A., E. Blinman, L. Tauxe, et al. 2021. "MagIC as a FAIR Repository for America's Directional Archaeomagnetic Legacy Data." *Journal of Geophysical Research: Solid Earth* 126, no. 10: e2021JB022874. https://doi.org/10.1029/2021JB022874.

Jones, S. A., L. Tauxe, E. Blinman, and A. Genevey. 2020. "Archeointensity of the Four Corners Region of the American Southwest." *Geochemistry, Geophysics, Geosystems* 21, no. 3: e2018GC007509. https://doi.org/10.1029/2018GC007509.

Koenigsberger, J. G. 1930. "Größenverhältnis von remanentem zu induziertem Magnetismus in Gesteinen; Größe und Richtung des Rremanenten Magnetismus." *Zeitschrift für Geophysik* 6: 190–207. https://doi.org/10.23689/fidgeo-3212.

Korte, M., F. Donadini, and C. G. Constable. 2009. "Geomagnetic Field for 0–3 ka: 2. A New Series of Time-Varying Global Models." *Geochemistry, Geophysics, Geosystems* 10, no. 6: Q06008. https://doi.org/10.1029/2008GC002297.

Lémuz Aguirre, C. 2024. "Prospección arqueológica en el Sector de Mollo Kontu—Tiwanaku." *Boletín de la Sociedad de Arqueología de La Paz—Bolivia* 1: 1–60. https://www.arqueobolivia.org/boletin-n1/.

Lengyel, S. N., J. L. Eighmy, and M. Van Buren. 2011. "Archaeomagnetic Research in the Andean Highlands." *Journal of Archaeological Science* 38, no. 1: 147–155. https://doi.org/10.1016/j.jas.2010.08.021.

Lizárraga, R. 1605/1916. *Descripción Breve de Toda la Tierra del Perú, Tucumán, Río de la Plata y Chile*. Vol. 2. Librería La Facultad, de Juan Roldán.

Macario, K. T., F. M. de Oliveira, I. S. Chanca, C. Carvalho, E. Q. Alves, and I. Pedroza. 2025. "Radiocarbon Dating in South America and the Impact of the Continent's First 14C-AMS Facility to Archaeological Research." *Archaeometry* 67: S141–S158. https://doi.org/10.1111/arcm.13055.

Macfarlane, A. W., and H. N. Lechtman. 2016. "Andean Ores, Bronze Artifacts, and Lead Isotopes: Constraints on Metal Sources in Their Geological Context." *Journal of Archaeological Method and Theory* 23, no. 1: 1–72. https://doi.org/10.1007/s10816-014-9225-8.

Marsh, E. J. 2012. "A Bayesian Re-Assessment of the Earliest Radiocarbon Dates From Tiwanaku, Bolivia." *Radiocarbon* 54, no. 2: 203–218. https://doi.org/10.2458/azu_js_rc.v54i2.15826.

Marsh, E. J. 2016. "Building Household and Community Through Active Assemblages: A Late Formative Patio Group at Khonkho Wankane, Bolivia." *Cambridge Archaeological Journal* 26, no. 2: 305–327. https://doi.org/10.1017/S0959774315000499.

Marsh, E. J., C. J. Harpel, and D. E. Damby. 2024. "The Khonkho Tephra: A Large-Magnitude Volcanic Eruption Coincided With the Rise of Tiwanaku in the Andes." *Holocene* 34, no. 12: 1865–1874.

Marsh, E. J., A. Korpisaari, S. Puerto Mundt, A. Gasco, and V. Durán. 2021. "Radiocarbon vs. Luminescence Dating of Archaeological Ceramics in the Southern Andes: A Review of Paired Dates, Bayesian Models, and a Pilot Study." *Radiocarbon* 63, no. 5: 1471–1501. https://doi.org/10.1017/RDC.2021.82.

Marsh, E. J., A. Vranich, D. Blom, et al. 2023. "The Center Cannot Hold: A Bayesian Chronology for the Collapse of Tiwanaku." *PLoS One* 18, no. 11: e0288798. https://doi.org/10.1371/journal.pone.0288798.

Maximiano, P. F., W. Poletti, G. L. Mathias, M. G. Rocha, and R. I. F. Trindade. 2024. "Towards the use of Archaeomagnetism as an Archaeological Dating Tool for South America." *Journal of South American Earth Sciences* 144: 105038. https://doi.org/10.1016/j.jsames.2024.105038.

Moya, J., and A. Lara. 2011. "Cronologías de Ancho de Anillos de Queñoa (*Polylepis tarapacana*) Para los Últimos 500 años en el Altiplano de la Región de Arica y Parinacota, Chile." *Bosque* 32, no. 2: 165–173. https://doi.org/10.4067/S0717-92002011000200007.

Palencia-Ortas, A., A. Molina-Cardín, M. L. Osete, et al. 2021. "Inclination Flattening Effect in Highly Anisotropic Archaeological Structures From Iberia. Influence on Aarchaeomagnetic Ddating." *Physics of the Earth and Planetary Interiors* 318: 106762. https://doi.org/10.1016/j.pepi.2021.106762.

Pavón-Carrasco, F. J., J. Rodríguez-González, M. L. Osete, and J. M. Torta. 2011. "A Matlab Tool for Archaeomagnetic Dating." *Journal of Archaeological Science* 38, no. 2: 408–419. https://doi.org/10.1016/j.jas.2010.09.021.

Poletti, W., R. I. F. Trindade, G. A. Hartmann, N. Damiani, and R. M. Rech. 2016. "Archeomagnetism of Jesuit Missions in South Brazil (1657–1706 AD) and Assessment of the South American Database." *Earth and Planetary Science Letters* 445: 36–47. https://doi.org/10.1016/j.epsl.2016.04.006.

Ponce Sanginés, C. 1976. *Tiwanaku: Espacio, Tiempo y Cultura. Ensayo de Síntesis Arqueológica*. 3rd ed. Ediciones Pumapunku.

Prévot, M., E. A. Mankinen, R. S. Coe, and C. S. Grommé. 1985. "The Steens Mountain (Oregon) Geomagnetic Polarity Transition: 2. Field Intensity Variations and Discussion of Reversal Models." *Journal of Geophysical Research: Solid Earth* 90, no. B12: 10417–10448. https://doi.org/10.1029/JB090iB12p10417.

Schiffer, M. B. 1986. "Radiocarbon Dating and the "Old Wood" Problem: The Case of the Hohokam Chronology." *Journal of Archaeological Science* 13, no. 1: 13–30. https://doi.org/10.1016/0305-4403(86)90024-5.

Serrano, M., F. J. Pavón-Carrasco, S. A. Campuzano, and M. L. Osete. 2024. "ArchaeoPyDating: A New User-Friendly Release for Archaeomagnetic Dating." *Archaeometry* 66, no. 6: 1424–1437. https://doi.org/10.1111/arcm.13009.

Solíz, C., R. Villalba, J. Argollo, et al. 2009. "Spatio-Temporal Variations in *Polylepis tarapacana* Radial Growth Across the Bolivian Altiplano During the 20th Century." *Palaeogeography, Palaeoclimatology, Palaeoecology* 281, no. 3: 296–308. https://doi.org/10.1016/j.palaeo.2008.07.025.

Stacey, F. D. 1967. "The Koenigsberger Ratio and the Nature of Thermoremanence in Igneous Rocks." *Earth Plant Science Letters* 2: 67–68. https://doi.org/10.1016/0012-821x(67)90174-4.

Tauxe, L, S. K. Banerjee, R. F. Butler and R. van der Voo. 2018. Essentials of paleomagnetism: 5th Web Edition. https://earthref.org/MagIC/books/Tauxe/Essentials/.

Thellier, E., and O. Thellier. 1959. "Sur l'intensité du champ magnétique terrestre dans le passé historique et geologique." *Annales Geophysicae* 15: 285–376.

Turner, G. M., R. Kinger, B. McFadgen, and M. Gevers. 2020. "The First Archaeointensity Records From New Zealand: Evidence for a Fifteenth Century AD Archaeomagnetic "Spike" in the SW Pacific Region?" *Geological Society, London, Special Publications* 497, no. 1: 47–72. https://doi.org/10.1144/SP497-2019-71.

Vodyasov, E. V., O. V. Zaitceva, M. V. Vavulin, and A. A. Pushkarev. 2020. "The Earliest box-Shaped iron Smelting Furnaces in Asia: New Data From Southern Siberia." *Journal of Archaeological Science: Reports* 31: 102383. https://doi.org/10.1016/j.jasrep.2020.102383.

Vranich, A. 2006. "The Construction and Reconstruction of Ritual Space at Tiwanaku, Bolivia (A.D. 500–1000)." *Journal of Field Archaeology* 31, no. 2: 121–136. https://www.jstor.org/stable/40024952.

Wolfman, D., and R. E. Dodson. 1998. "Archaeomagnetic Results From Peru: AD 700–1500." *Andean Past* 5, no. 1: 20. https://digitalcommons.library.umaine.edu/andean_past/vol5/iss1/20.

Supporting Information

Additional supporting information can be found online in the Supporting Information section. **Table S1:** List of all samples, specimens, and experiments that comprise the study. "Sample ID" refers to samples retrieved during fieldwork, as shown in Figure 1 in the main text. "Specimen ID" refers to each 2-cm^3 cube. For ease of manipulation, each specimen is attributed a correlative number, their "Lab ID." "Experiment" indicates whether the specimen has undergone Thellier–Thellier archaeointensity determination (AI) or stepwise thermal demagnetization (ThD). **Table S2:** Rock-magnetic parameters. Lab ID as in Table SI1; Bcr: remanent coercive field; S: saturation at 300 mT; Ms.: saturation magnetization; Mrs.: remanent saturation magnetization; Bc: coercive field; TC: Curie temperatures. **Figure S1:** Rock magnetism graphs for selected specimens. a) IRM acquisition curve; b) backfield curve; c) hysteresis loop; d) thermomagnetic curve. Figure continued below. **Figure S2:** A sequence showing the two phases of a standard Thellier–Thellier step and the six extra phases performed at the same temperature used for anisotropy (a) and cooling rate (b) corrections. Note that TRMani corrections are based on the comparison between the measurements in different axes, while the CR is based on the speed of cooling (quick vs. slow). **Table S3:** Quality criteria used in archaeointensity calculations, including the minimum or maximum acceptable value in each case. **Figure S3:** Archaeointensity graphs for the specimens not shown in main text. Arai (intensity) plots for specimens belonging to different samples, including their related Zijderveld (directional) plots at the upper right corner. Red line in the Arai and Zijderveld plot marks the sequence of temperature steps used in intensity and directional calculations; gray arrows mark the pTRM checks. The values of the obtained intensity at the specimen level corrected for anisotropy and cooling rate effects (Bac) and the quality parameter (q) are provided, alongside the initial NRM values. **Table S4:** Archaeointensity data at the specimen level, with site mean intensity below. Sample: field sample to which the specimens belong to Lab ID: correlative number identifying the specimen (see Table SI for more information); T1 and T2: minimum and maximum temperatures used for archaeointensity (slope) calculation; n1: number of temperature steps between T1 and T2; f: fraction of NRM used in the calculation; g: gap factor; q: quality factor; k: Arai plot curvature parameter; β: ratio between the standard error and the absolute value of the slope; MAD: maximum angle of deviation; DANG: deviation angle; B: archaeointensity; f_ani: anisotropy correction factor; Ba: archaeointensity after TRM anisotropy correction; f_CR: cooling rate correction factor; Bac: archaeointensity after TRM anisotropy and cooling rate corrections; CR: cooling rate; CR_evol: evolution of the cooling rate. **Figure S4:** Representative demagnetization plots for different samples. Each specimen includes the intensity of the initial NRM. Its Zijderveld plot is displayed on the left; open circles represent the vertical and full circles the horizontal components of the magnetic vector. On the upper right of each specimen, its stereogram with the mean direction of the specimen represented as a full burgundy circle; note that all inclinations are negative, as corresponding to the Southern Hemisphere. On the lower right, the intensity decay plot corresponding to each demagnetization step. **Table S5:** Directional data at the specimen level. Sample and Lab ID as in previous table; T1 and T2: minimum and maximum temperatures for directional calculation; n1: number of steps between T1 and T2; D: declination calculated through origin, without anisotropy correction; I: inclination calculated through origin, without anisotropy correction; MAD: maximum angle of deviation calculated through origin, without anisotropy correction; D_cor: declination calculated through origin, corrected for anisotropy and cooling effects (only in specimens that underwent Thellier–Thellier); I_cor: inclination calculated through origin, corrected for anisotropy and cooling rate effects (only in specimens that underwent Thellier–Thellier); MAD_cor: maximum angle of deviation calculated through origin, corrected for anisotropy and cooling rate effects (only in specimens that underwent Thellier–Thellier); Experiment: AI—archaeointensity by Thellier–Thellier, ThD—stepwise thermal demagnetization. **Table S7:** Final data obtained from the furnace, both uncorrected and corrected for anisotropy and cooling rate effects. n/N: number of specimens/number of field samples; D: declination; I: inclination; $\alpha 95$: semi-angle of 95% confidence (Fisher, 1953); B: intensity; σB: standard deviation (error) of the intensity. Note that the intensity values are calculated as a weighted mean (Prevot et al., 1985). **Figure S5:** Dating results from different models and curves at 95%. **Figure S4:** Dating results from different models and curves at 68%. **Data S1:** Supporting Information.